

RESEARCH ARTICLE

Energetics and thermodynamic stability of potential Fe^(II)-hexa-aza-active sites for O₂ reduction in PEM fuel cells

Vassili P. Glibin¹  | Jean-Pol Dodelet²  | Gaixia Zhang^{2,3} 

¹Department of Chemical and Biochemical Engineering, University of Western Ontario, London Ontario, Canada

²Institut National de la Recherche Scientifique (INRS), Énergie Matériaux Télécommunications Research Centre, Varennes, Quebec, Canada

³Department of Electrical Engineering, École de Technologie Supérieure (ÉTS), 1100, rue Notre-Dame Ouest, Montréal, Québec H3C 1K3, Canada

Correspondence

Vassili P. Glibin, Department of Chemical and Biochemical Engineering, University of Western Ontario, London, N6A 5B9, Canada.

Email: vassili.glibin@gmail.com

Jean-Pol Dodelet, Institut National de la Recherche Scientifique (INRS), Énergie Matériaux Télécommunications Research Centre, Varennes, Quebec J3X1P7, Canada.

Email: jean-pol.dodelet@inrs.ca

Gaixia Zhang, Department of Electrical Engineering, École de Technologie Supérieure (ÉTS), Montréal, Québec H3C 1K3, Canada.

Email: gaixia.zhang@etsmtl.ca

Abstract

We present here a thermodynamic assessment of the stability behavior in acid environment at 298 and 353 K (80°C) of two iron (II) hexa-aza-macrocylic complexes and of an hexa-aza-iron-based site (Fe^{II}N₍₄₊₂₎/C) that should potentially be active for the oxygen reduction reaction in proton exchange membrane (PEM) fuel cells. The calculations of the equilibrium constant (K_c) for the demetallation reaction indicate that the iron (II)-hexa-aza-macrocylic complexes and Fe^{II}N₍₄₊₂₎/C are chemically stable in an acid medium at 298 and 353 K. Compared with two other potential model sites (Fe^{II}N₄/C and Fe^{II}N₍₂₊₂₎/C) that were thought to be present in the same Fe-based catalysts, K_c of Fe^{II}N₍₄₊₂₎/C is two to three orders of magnitude smaller at 353 K, and three to four orders of magnitude smaller at 298 K, than K_c for Fe^{II}N₄/C or Fe^{II}N₍₂₊₂₎/C, revealing the great chemical stability of Fe^{II}N₍₄₊₂₎/C. In this work, we discuss about a novel proposition that the two catalytic sites active in these Fe-based catalysts are Fe^{II}N₄/C and Fe^{II}N₍₄₊₂₎/C. This proposition is in agreement with the durability behavior of these catalysts in PEM fuel cells and also with their known physico-chemical characterizations. The origin of the fast and slow decay behaviors of the different sites, which are active at the Fe–N–C-based cathode of PEM fuel cells, is also discussed.

KEYWORDS

active site, fuel cell, oxygen reduction reaction, thermodynamic stability

1 | INTRODUCTION

In recent years, the so-called “single-atom” electrocatalysts have received increased attention due to their relatively high electrochemical activity for the reaction of molecular oxygen reduction reaction (ORR). Practically, all the studies were focused on the first four coordinating N-atoms of the MetalN₄ sites. The family of coordination compounds

of transition metals with hexa-aza-macrocylic ligands is also of great interest due to its enhanced stability with regard to the electrolytic dissociation, their ability to catalyze various chemical reactions and, in electrochemistry, to catalyze the ORR,^{1,2} the reduction of H₂O to H₂ and of CO₂ to CO and/or formic acid.^{3,4} In our previous work,⁵ we showed that the initial fast decrease in the activities of porphyrin-like (FeN₄/C) and 1,10-phenanthroline

This is an open access article under the terms of the [Creative Commons Attribution](https://creativecommons.org/licenses/by/4.0/) License, which permits use, distribution and reproduction in any medium, provided the original work is properly cited.

© 2022 The Authors. *SusMat* published by Sichuan University and John Wiley & Sons Australia, Ltd.

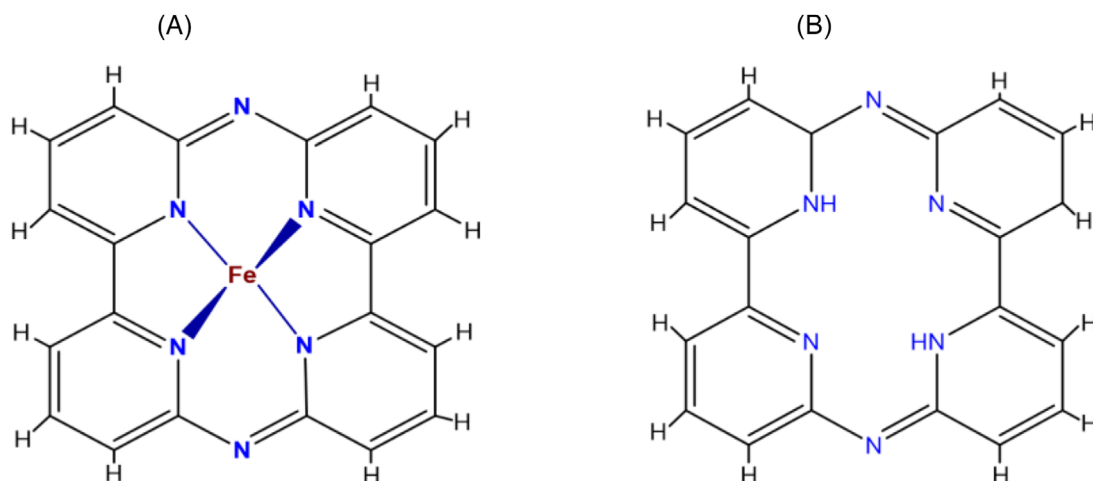


FIGURE 1 Iron (II) complex with hexa-aza-macrocyclic ligand having 2,2'-bipyridine groups: $\text{FeN}_4[\text{C}_{20}\text{N}_2\text{H}_{12}]$ (A) and its demetallated form: $\text{H}_2\text{N}_4[\text{C}_{20}\text{N}_2\text{H}_{12}]$ (B). \blacktriangleright is the symbol of the donor–acceptor bond

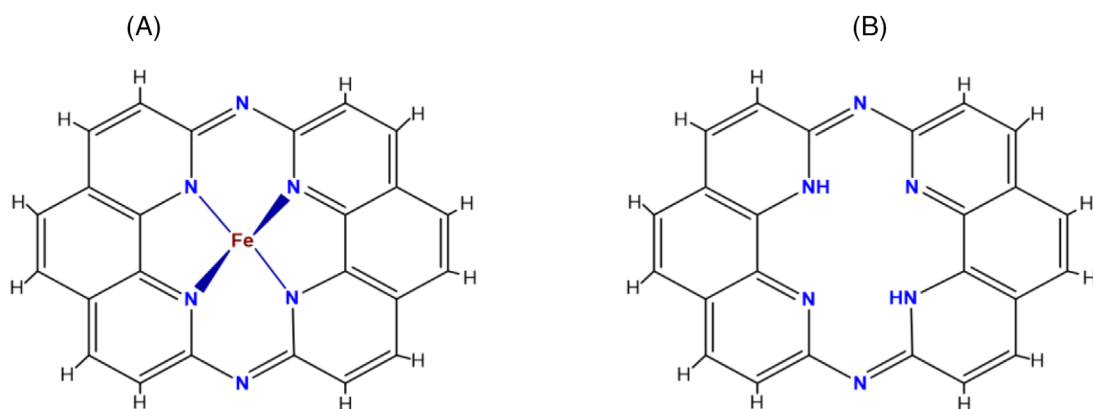


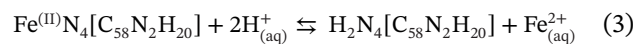
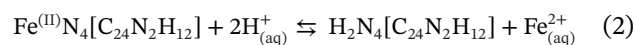
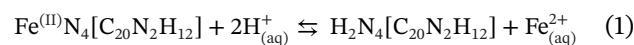
FIGURE 2 Iron (II) complex with hexa-aza-macrocyclic ligand having 1,10-phenanthroline groups: $\text{FeN}_4[\text{C}_{24}\text{N}_2\text{H}_{12}]$ (A) and its demetallated form: $\text{H}_2\text{N}_4[\text{C}_{24}\text{N}_2\text{H}_{12}]$ (B). \blacktriangleright is the symbol of the donor–acceptor bond

(Phen)-like ($\text{FeN}_{(2+2)}/\text{C}$) electrocatalytic centers in the molecular ORR in the acid medium of PEM fuel cells is most likely due to iron ions leaching from sites located in the micropores of the Fe–N–C catalyst (a demetallation reaction). Furthermore, we believe now that the true structure of $\text{FeN}_{(2+2)}/\text{C}$ is probably more related to the structure of iron (II) complexes with hexa-aza-macrocyclic ligands, as illustrated in Figures 1A and 2A, being embedded into a graphene layer (Figure 3A) of Fe-based catalysts obtained by high-temperature pyrolysis of iron, nitrogen, and carbon precursors. Due to their structural analogy with the well-studied FeN_4/C electrocatalytic sites, these hexa-aza $\text{FeN}_{(4+2)}/\text{C}$ sites, as we will name them, should most probably display an ORR electrochemical activity and have a better resistance to iron acid leaching than FeN_4/C also found in the same catalysts.

The molecular structure $\text{FeN}_{(4+2)}/\text{C}$ (shown in Figure 3A) is a $\text{FeN}_{(4+2)}$ site inserted into a graphene layer for which the iron (II) complex is an hexa-aza-

macrocyclic ligand with Phen grouping. $\text{FeN}_{(4+2)}/\text{C}$ was modeled using the molecular structure of Figure 2A with covalently bonded carbon hexagons. The vacant valences of the terminal carbon atoms in the molecular model are saturated by hydrogen atoms. For this example of $\text{FeN}_{(4+2)}/\text{C}$ and the iron-free framework, $\text{H}_2\text{N}_{(4+2)}/\text{C}$, the used molecular formulas are as follows: $\text{FeN}_4[\text{C}_{58}\text{N}_2\text{H}_{20}]$ (Figure 3A) and $\text{H}_2\text{N}_4[\text{C}_{58}\text{N}_2\text{H}_{20}]$ (Figure 3B), respectively.

For the reactions of demetallation (iron acid leaching), we can write:



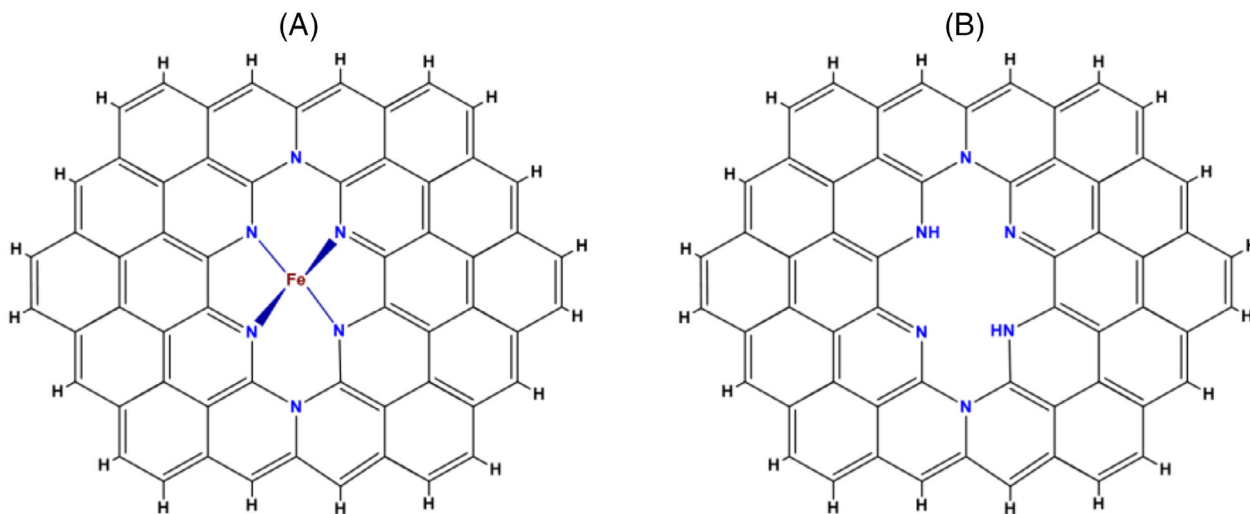


FIGURE 3 Molecular models of $\text{FeN}_{(4+2)}/\text{C}$ or $(\text{Fe}^{\text{II}}\text{N}_4[\text{C}_{58}\text{N}_2\text{H}_{20}])$ electrocatalytic site (A) and its demetallated form $\text{H}_2\text{N}_{(4+2)}/\text{C}$ (or $\text{H}_2\text{N}_4[\text{C}_{58}\text{N}_2\text{H}_{20}]$) (B). \blacktriangleright is the symbol of the donor-acceptor bond

where the symbols $\text{H}^+_{(\text{aq})}$ and $\text{Fe}^{2+}_{(\text{aq})}$ refer to the hydrogen and iron (II) ions in solution; $\text{Fe}^{\text{II}}\text{N}_4[\text{C}_{20}\text{N}_2\text{H}_{12}]$ and $\text{Fe}^{\text{II}}\text{N}_4[\text{C}_{24}\text{N}_2\text{H}_{12}]$ are the iron (II) complexes with hexa-aza-macrocyclic ligands of Figures 1A and 2A, respectively; $\text{Fe}^{\text{II}}\text{N}_4[\text{C}_{58}\text{N}_2\text{H}_{20}]$ is the modeled electrocatalyst site $\text{FeN}_{(4+2)}/\text{C}$ of Figure 3A; $\text{H}_2\text{N}_4[\text{C}_{20}\text{N}_2\text{H}_{12}]$, $\text{H}_2\text{N}_4[\text{C}_{24}\text{N}_2\text{H}_{12}]$, and $\text{H}_2\text{N}_4[\text{C}_{58}\text{N}_2\text{H}_{20}]$ (or $\text{H}_2\text{N}_{(4+2)}/\text{C}$) are the demetallated forms of Figures 1B, 2B, and 3B, respectively.

To quantitatively estimate the extent of such reactions, we will use the values of equilibrium constants, K_c , determined as follows:

$$\ln K_c = \frac{-\Delta_r G_T^0}{RT} \quad (4)$$

where $\Delta_r G_T^0$ is the Gibbs free energy of Reactions (1)–(3), R is the universal gas constant, and T is the temperature in K. In turn, to determine the Gibbs free energy of Reactions (1)–(3) at temperature T , the following equation can be used⁶:

$$\Delta_r G_T^0 = \Delta_r H_{298}^0 - T\Delta_r S_{298}^0 + \Delta C_{p,298} \times \left[(T - 298) - T \ln \left(\frac{T}{298} \right) \right] \quad (5)$$

where $\Delta_r H_{298}^0$, $\Delta_r S_{298}^0$, and $\Delta C_{p,298}$ are the standard enthalpy, standard entropy, and heat capacity changes, at 298 K, in Reactions (1)–(3), respectively. The enthalpy change, $\Delta_r H_{298}^0$, is calculated as the difference between the standard enthalpies of formation of the product and reactant parts of these reactions. The values of $\Delta_r S_{298}^0$

and $\Delta C_{p,298}$ can be determined analogously. In our case, given the small value of the difference between 353 K (the usual temperature of a running PEM fuel cell) and 298 K, the last term ($\Delta C_{p,298} \times [(T - 298) - T \ln(T/298)]$) in Equation (5) may be neglected. Standard entropies and enthalpies of formation of $\text{H}^+_{(\text{aq})}$ and $\text{Fe}^{2+}_{(\text{aq})}$ ions are tabulated.⁷ Since the data on standard enthalpies of formation of the frameworks of Reactions (1)–(3) are absent, we used N–H and Fe–N bonds energies (along with tabulated standard enthalpies of formation of $\text{H}^+_{(\text{aq})}$ and $\text{Fe}^{2+}_{(\text{aq})}$ ions) to calculate the enthalpy change of these reactions.

The correct determination of equilibrium constants using bond energies implies the determination of Fe–N and N–H bond energies with a so-called “chemical accuracy,” that is, within the uncertainty of an order of 5 kJ mol⁻¹. Even though the quantum-chemical methods (ab initio and based on density functional theory) are currently widely used for investigating molecular electronic structures, interatomic distances, and chemical bond energies, the semi-empirical and empirical methods have also their own merits: rapid calculations, enough accuracy, and wide applicability. The latest developments in the electronegativity concept have led to relatively simple methods for the determination of molecular properties such as the charge distribution in simple and large molecules,^{8–21} interatomic distances,^{20–22} chemical bonds energy,^{20–21,23–26} proton affinity,^{20,27} force constants,^{19,28} dipole moments,²⁹ and other properties. In this work, the previously developed semi-empirical methods (relying on the concept of electronegativity) are used for computing interatomic distances and Fe–N bond energies.

2 | CONCEPT OF ELECTRONEGATIVITY IN THE DETERMINATION OF Fe–N INTERATOMIC DISTANCES AND Fe–N BOND ENERGIES IN IRON (II) COMPLEXES WITH HEXA-AZA-MACROCYCLIC LIGANDS AND THE MODELED $\text{FeN}_{(4+2)}/\text{C}$ ELECTROCATALYST

2.1 | Modeling of Fe–N bond energies

Ferreira,³⁰ Evans and Huheey,³¹ and Urusov³² showed that the bond energy can be modeled as the sum of the three contributing terms into total energy. They are: the covalent contributing term (first term in Equation 6) due to the overlap of bonding orbitals of atoms forming a bond, the energy of the electrostatic interaction (second term in Equation 6) due to an attraction of opposite partial charges on atoms forming a bond, and the energy associated with the charge transfer from a metal atom to a ligand (third term in Equation 6). The bond energy can be represented by the following equation:

$$E \text{ (eV)} = (1 - i^2)^{1/2} D_0 + \frac{e_0^2 i}{d} (1 - n^{-1}) + \Delta E \quad (6)$$

where i is the bond ionicity (fractional ionic character of a bond), D_0 is the covalent energy, related to Pauling's geometric mean³³ but allowing for a decreasing overlap with an increasing ionicity, e_0 is the electron charge, n is the Born exponent, a number between 5 and 12, d is the interatomic distance, and ΔE is the charge transfer affinity term,³⁴ which is the energy resulting from the transfer of electron density from a less electronegative atom to a more electronegative one. As can be seen from Equation (6), the first two contributions into the bond energy are functions of i ; with increasing the ionicity of the bond, the covalent first term in Equation (6) decreases, and the second term in Equation (6) increases.

The second term in Equation (6) corresponds to the electrostatic contribution into a bond energy due to the partial charges appearing on the atoms. The Born exponent appears in the $1/d^n$ dependence of the repulsive interaction resulting from the electron–electron repulsions between two electronic shells of atoms.³⁵ Following Ferreira's suggestion,³⁰ we accepted in our calculations the n value equal to 9. The methods used for the determination of Fe–N bonds ionicity, Fe–N interatomic distances, and the ΔE term are presented in Supporting Information.

Since the determination of Fe–N interatomic distances in this work is based on the use of partial charges on atoms (see the Bergman-Hinze equation, Supporting Information, Equation A5), we consider it necessary to provide the description of an approach used in this work for the

assessment of partial charges of atoms in the FeN_4 groupings. It is presented as the combination of two methods; the first one is based on Sanderson's principle of full equalization of electronegativities of atoms in a molecule³⁶ and the second³⁷ is based on the averaging partial charges, calculated for each bond involving the atom for which the partial charge will be determined considering that each pair of bonded atoms in a complex structure behaves like a separate diatomic molecule (the so-called Pauling type of calculations).

2.2 | Short description of methods used for the assessment of partial charges on atoms

For the first method, the principle of full electronegativity equalization upon bond formation formulated by Sanderson³⁶ states that when molecules are formed, the electronegativities of the all-constituent atoms become equal. Parr et al.³⁸ have found quantum-mechanical support for Sanderson's principle. To calculate the charge of an atom, one should first calculate, according to Sanderson, the equalized electronegativity, χ_{eq} , of all the atoms in a molecule, which is determined as the geometric mean of the electronegativity values of each of the atoms, χ_i , in the molecule:

$$\chi_{\text{eq}} = \sqrt[n]{\prod_{i=1}^n \chi_i} \quad (7)$$

The partial charge (δ_i) acquired by any bonded atom is determined as follows:

$$\delta_i = \frac{\chi_{\text{eq}} - \chi_i}{1.57 \sqrt{\chi_i}} \quad (8)$$

However, a problem arises with this method when one has to calculate the partial charges of oxygen atoms in a molecule like acetic acid, CH_3COOH , for example. For this molecule, according to Sanderson's principle, oxygen atoms must have, regardless of their chemical nonequivalence, the same equalized electronegativity and, correspondingly, the same partial charge. To avoid this problem, Carver et al.³⁹ proposed a modified Sanderson's method. In the modified Sanderson's method, a molecule is considered as being composed of an ensemble of subgroups, rather than as an ensemble of atoms. A chemical subgroup is defined as any atom or group of atoms bonded directly to the atom of interest, which is considered as a central atom. The equalized electronegativity of a subgroup is calculated as the geometric mean of electronegativity of the constituent atoms.

The second method,³⁷ as we believe, is also well suited to calculate the partial charge of a central atom in coordination compounds. It has been shown in Ref. [37] that to adapt Pauling type of calculations to molecules containing more than one bond, it is necessary to add the arithmetic average of partial charges of the first coordination sphere of the atom for which the partial charge is being calculated to the reduced average of the second coordination sphere. The effect of the second coordination sphere is taken into account by multiplying the obtained partial charges of the first coordination sphere by an empirical factor. Finally, the multiplicity of bonds associated with the considered atom can be accounted by using the multiple bond factor. The partial charge of a central atom A (δ_A) then is calculated as a function of Δ , as follows³⁷:

$$\Delta = \chi_A - \frac{\sum_i R_i \chi_i + \Omega \sum_j R_j \chi_j}{1 + \sum_i R_i + \sum_j R_j} \quad (9)$$

$$\delta_A = \frac{\Delta}{1.57 \sqrt{\chi_A}} \quad (10)$$

where Δ is the difference between the electronegativity of the atom A (χ_A) (for which the partial charge is being calculated) and the sum of the averaged electronegativity (χ_i) of i th atoms of the first coordination sphere of atom A and the reduced averaged electronegativity (χ_j) of the j th atoms forming the second coordination sphere. R_i is the multiple bond factor associated with the considered atom (which was found equal to 1.2 for double bonds) and Ω is the weighting factor for the second coordination sphere of atom A (given that $\Omega = 0.2$).³⁷

In Ref. [37] it was established that the best correlation between partial charges on atoms and the data of X-ray photoelectron study of electrons binding energy (electron spectroscopy for chemical analysis) is observed if one uses the linear combination of the charges obtained using both methods, more specifically calculated as the sum of the amount of 60% of data obtained using the modified Sanderson method and, correspondingly, of the amount of 40% of the data obtained using the Pauling type calculations (the second method).

2.3 | Computations and results of Fe–N interatomic distances and Fe–N bond energies determination in iron (II) complexes with aza-macrocyclic ligands and the modeled electrocatalyst

Although electronegativity, as it was emphasized by Huheey et al.,⁴⁰ is often treated as an invariant prop-

erty, it actually depends upon a number of factors such as the valence and oxidation states of the atom, the charge on the atom (either an integral charge as an ion or a partial charge as an atom in a molecule), and the hybridization of the atom. Hybridization affects electronegativity due to the reason that orbitals of atoms having greater s-character are more electronegative.⁴⁰ Applying the modified Sanderson's method, we have used the Sanderson's scale.⁴¹ In the case of application of the second method, the well-known Pauling's scale (Table 3.12 in Ref. [40]) was used. These scales are based on different physical principles of the electronegativity definition, and therefore they have different units and differing values, although the values of electronegativities of atoms of these scales correlate well among themselves. The values of electronegativity and hardness of atoms and ions (on the Mulliken scale of electronegativity⁴²) in their different valence states were obtained from Refs. [43]–[46]

Thus, using the modified Sanderson's method, it was obtained from Equations (7) and (8) that Fe- and N-atom partial charges (in electron units, e.u.) in each FeN₄ grouping of iron (II) complexes and the modeled electrocatalyst are equal to +0.555 (for the iron atom) and –0.156 (for each of the four nitrogen atoms) in Figures 1A–3A. The application of the second method (Pauling type calculations: Equations 9 and 10) gave the values of the partial charge of Fe-atoms in iron (II) complexes and the modeled electrocatalyst equal to +0.508 for Figure 1A, +0.519 for Figure 2A, and +0.573 for Figure 3A, respectively. In these calculations, the first coordination sphere of iron atoms in both complexes (Figures 1A and 2A) and in the modeled electrocatalyst (Figure 3A) was considered consisting of four atoms of nitrogen and the second sphere was considered as composed of all the remaining atoms. The multiple bonding factor for Fe–N and C–N bonds in Figures 1A–3A was adopted equal to 1.1, that is, the value intermediate between 1 (ordinary bonds) and 1.2 (double bonds); and for C–H bonds, it was taken equal to 1. It is interesting to note that the obtained partial charges of iron atoms in iron (II) complexes and in the modeled electrocatalyst are close to the δ_{Fe} value of +0.521; the value obtained by substitution of electronegativities of iron atoms (1.83 eV^{1/2}, Table 3.12 in Ref. [40]) and a pyridine molecule (1.42 eV^{1/2}, the converted value of 4.4 eV⁴³) into Equation (A2), assuming that hexa-aza ligands and pyridine molecules have to some extent similar behavior as complex-forming species. This fact indicates a good enough reliability of the above-estimated partial charges of iron atoms. The necessary conversion of electronegativities of pyridine, $\chi_{Mulliken}$, from Mulliken's units (eV), into Pauling's units, χ_P (eV^{1/2}), was carried out using the following modification⁴⁷ of the

TABLE 1 Partial charges (δ) of Fe- and N-atoms, Fe–N interatomic distances ($d_{\text{Fe–N}}$), and Fe–N bond energies ($E_{\text{Fe–N}}$) in iron (II) hexa-aza-macrocyclic complexes and the modeled electrocatalyst in comparison with the data on Fe–N interatomic distances and Fe–N bond energies for already studied electrocatalysts

Compound, electrocatalyst	$\delta_{\text{Fe}}^{\text{a}}$ (e.u.)	$\delta_{\text{N}}^{\text{a}}$ (e.u.) (estimated value) ^b	$d_{\text{Fe–N}}$ (Å), Equation (A5)	$E_{\text{Fe–N}}$ (kJ mol ^{−1}), Equation (6)
Fe ^(II) N ₄ [C ₂₀ N ₂ H ₁₂]	+0.536	−0.13 ₄	2.00 ± 0.03	219.4 ± 5 (<i>i</i> = 0.156) ^c
Fe ^(II) N ₄ [C ₂₄ N ₂ H ₁₂]	+0.541	−0.13 ₅	2.00 ± 0.03	219.4 ± 5 (<i>i</i> = 0.156) ^c
Fe ^(II) N ₄ [C ₅₈ N ₂ H ₂₀] (electrocatalyst modeled in this work, Fe ^(II) N ₍₄₊₂₎ /C)	+0.562	−0.14	1.99 ₅ ± 0.03	221.4 ± 5 (<i>i</i> = 0.160) ^c
Fe ^(II) N ₍₂₊₂₎ /C (FeN ₄ C ₆₀ H ₂₀ ; “armchair” electrocatalyst) ^d	+0.537 ^e	−0.13 ₄	2.00 ± 0.03 1.97 ± 0.03 ^d	216.3 ± 5 (<i>i</i> = 0.150) ^c 216.7 ± 5 ^f
Fe ^(II) N ₄ /C (FeN ₄ C ₆₂ H ₂₂ ; “zig-zag” electrocatalyst) ^d	+0.538 ^e	−0.13 ₄	2.00 ± 0.03 1.98 ± 0.03 ^g	216.3 ± 5 (<i>i</i> = 0.150) ^c 213.5 ± 5 ^f

^a δ is (in contrast to the charge of an ion) a non-integer charge value created by the asymmetrical distribution of electrons in chemical bonds and measured in elementary charge units.

^bPrinciple of electroneutrality applied to the first coordination sphere.

^cThe value of Fe–N bond ionicity used in our calculations with Equation (6).

^dRef. [50]

^eCalculated using the modified Sanderson method, namely, considering the modeled electrocatalyst as an ensemble of two groupings: FeN₄C₂₆ and C₃₄H₂₀ in the case of “armchair” electrocatalyst, and FeN₄C₂₂ and C₄₀H₂₂ in the case of “zig-zag” electrocatalyst.

^fCalculated using the following equation: $E_{\text{Fe–N}}$ (kJ mol^{−1}) = 1657/ $d_{\text{Fe–N}}^3$, Ref. [50]

^gRef. [49]; X-ray absorption near-edge spectroscopy (XANES) data.

original Bratsch’s formula⁴⁵:

$$\chi_{\text{P}} = 1.934\sqrt{\chi_{\text{Mulliken}} + 7.02} - 5.12 \quad (11)$$

The observed little discrepancy between partial charges of iron atoms calculated using both methods is seemingly caused by the fact that the chemical nonequivalence of the same atoms is not fully taken into account in the modified Sanderson’s method. To account for it, we specified the values of δ_{Fe} in both iron (II) complexes and the modeled electrocatalyst (Table 1) by the use of the linear combination (Sanderson 60%/Pauling 40%) of calculated charges obtained using both methods as previously described at the end of the Section 2.2.

Further, by substitution of partial charges, covalent radii of iron and nitrogen (1.32 and 0.71 Å, respectively⁴⁸), and hardness of iron and nitrogen atoms (ions) into Equation (A5) (Supporting Information), the interatomic distances, $d_{\text{Fe–N}}$, in iron (II) hexa-aza-macrocyclic complexes and the modeled electrocatalyst were determined (Table 1). The following data on the hardness of iron and nitrogen atoms (ions) were used: $\eta_{\text{Fe}^{2+}} = 7.24$ ⁴³ and η_{N} (sp² hybridization) equal to 15.0 eV.⁴⁴ We note that the calculated Fe–N interatomic distances are close to the X-ray absorption near-edge spectroscopy (XANES) data of the same distances in other kinds of electrocatalysts^{49,50} not containing

nitrogen atoms in their iron atoms’ second coordination sphere.

Following the approach presented in Equation (6), the value of D_0 for the covalent bond energy of Fe–N in the first term of Equation (6) was determined as the geometric mean of the ordinary bond energies for Fe–Fe (100.0 kJ mol^{−1})⁵¹ and N–N (163.2 kJ mol^{−1}).⁵² Hence, D_0 was assessed to be equal to 127.7 kJ mol^{−1}.

The ionicity of N → Fe²⁺ donor–acceptor bond necessary to calculate the first and second terms of Equation (6) was determined by two methods; namely, using Equations (A3) and (A4) in Supporting Information. The application of these methods yielded the values of ionicity of 0.123 and 0.150, respectively; the latter value taken with minus sign is close to the partial charge of N-atoms (−0.156) obtained using the modified Sanderson’s method. In the calculation of N → Fe²⁺ donor–acceptor bond ionicity (Equation A3), $\chi_{\text{N}} = 11.78$ eV⁴⁵ (sp² hybridization of N-atoms), $\chi_{\text{Fe}^{2+}} = 7.86$ eV¹⁸ (Fe²⁺ ion coordinated to N-atoms in ligands), and the above indicated values of the hardness of atoms (ions) were used. In the calculation of the bond ionicity by Equation (A4), the values of $I_{\text{D}} = 9.3$ eV (potential ionization of a pyridine molecule) and $E_{\text{A}} = 12.58$ eV (electron affinity of Fe-atoms, dsp² hybridization) were taken from Refs. [43, 46] respectively.

Undoubtedly, an ionicity value of the order of 0.15, which is theoretically substantiated, should be used in

the determination of the first and second terms in Equation (6). This is true for electrocatalysts that do not have nitrogen atoms in the second coordination sphere. In our case, due to the more pronounced ability of nitrogen atoms to attract electrons toward themselves compared to carbon atoms ($\chi_N > \chi_C$), the electron density in the conjugated π -system of carbon-carbon bonds (see Figure 3) is redistributed, involving also in this process the iron-nitrogen bonds. As consequence, it leads, as we believe, to some increase of the ionicity of Fe-N bonds. Such considerations are in line with the results of MATLAB simulations of the electrical field in electrocatalysts showing that, due to the N-induced charge redistribution, the pristine electrical field in the FeN₄ grouping increases.⁵³ Accordingly, the values of the Fe-N bond ionicity (i) for the modeled electrocatalysts were appropriately adjusted, and are reported in column 5 of Table 1.

For the third term in Equation (6), we obtained by substitution of the above indicated data on electronegativity and hardness of atoms (ions) into Equation (A6), that the charge transfer affinity, ΔE , is of the order of 0.173 eV (16.7 kJ mol⁻¹).

Then, by summing all three terms in Equation (6), Fe-N bond energies in the studied complexes and in the modeled electrocatalyst were determined and summarized in Table 1 (column 5).

For comparison, we also recalculated, using this semi-empirical approach, the former values of the Fe-N bond energy⁵⁰ in the “armchair” and “zig-zag” electrocatalysts inserted into graphene (see the two last entries of $E_{\text{Fe-N}}$ in Table 1). As can be seen from Table 1, the application of this approach yielded values of Fe-N bond energies very close to those which were previously estimated, using a correlation equation of the type “interatomic distances versus bonds energy” (footnote “f” of Table 1) and taking into account XANES data⁴⁹ for Fe-N distances that were already experimentally determined for these electrocatalysts.

It is also seen from Table 1 that the presence of nitrogen atoms in the second coordination sphere of the modeled electrocatalyst increases the energy of Fe-N bonds compared with the energy of the Fe-N bonds of the “armchair” and “zig-zag” electrocatalysts. Although the difference between Fe-N binding energy in the hexa-aza electrocatalyst simulated in this work and that of the previously studied electrocatalysts is only of the order of 4 kJ mol⁻¹, given that this value is multiplied by 4 in the calculation of the reaction enthalpy (Equation 12), the resulting value, nevertheless, noticeably affects the Gibbs free energy of the demetallation reaction (see Equations 5 and 4) and, accordingly, the equilibrium constant value of the hexa-aza catalyst.

3 | THERMODYNAMIC CALCULATIONS

When Reactions (1)–(3) occur, four Fe-N bonds are broken and two N-H bonds are formed. Thus, we can write the following expression to estimate the enthalpy change, $\Delta_r H_{298}^0$, of these reactions:

$$\Delta_r H_{298}^0 = \left[\Delta_r H_{298}^0 \text{Fe}_{(\text{aq})}^{2+} + (-2E_{\text{N-H}}) \right] - \left[\Delta_r H_{298}^0 \text{H}_{(\text{aq})}^+ + (-4E_{\text{Fe-N}}) \right] \quad (12)$$

where $E_{\text{N-H}}$ and $E_{\text{Fe-N}}$ are the bond energies (more specifically, bond enthalpies), and $\Delta_r H_{298}^0 \text{Fe}_{(\text{aq})}^{2+}$ and $\Delta_r H_{298}^0 \text{H}_{(\text{aq})}^+$ are the standard enthalpies of formation of the ions in an aqueous solution. Note that the values of Fe-N bond energy have already been determined (see Table 1). The required value of N-H bond energy in the demetallated (base) frameworks (Figures 1B–3B) can be assessed using the following correlation equation⁵⁴:

$$E_{\text{N-H}} (\text{kJ mol}^{-1}) = 418.8 - 18.35\chi_C + 1.59\chi_C^2 = 382.3 \quad (13)$$

where χ_C is the Pauling electronegativity of a carbon atom (2.55) bonded to a nitrogen atom. Considering Equation (5), it is seen that along with data on the enthalpy change of Reactions (1)–(3), data on the entropy change are also required. The values of standard entropy of ions are tabulated,⁷ but the data on standard entropies of the frameworks appearing in Figures 1–3 are absent in the literature. We have used the following correlation equation of Glasser and Jenkins for the assessment of missing entropy values⁵⁵:

$$S_{298}^0 (\text{JK}^{-1} \text{mol}^{-1}) = 774 V_m (\text{nm}^3 / \text{per molecule}) + 57 \quad (14)$$

where V_m is the molecular volume. According to this method, the volume, V_m , can be assessed by summation of atomic contributions taken from Ref. [56] The use of Equation (14) permits to estimate the standard entropy of organic compounds with an error of the order of 5%. The impact of such error on values of the entropy changes of the Reactions (1)–(3) is low, since the same method is used in the estimations of S_{298}^0 of the product and reactant parts of these reactions. Results of the assessment of molecular volumes and standard entropies for iron (II) complexes, modeled electrocatalyst, and their demetallated forms are summarized in Table 2; the values of thermodynamic

TABLE 2 Estimated molecular volumes (V_m) and standard entropies (S_{298}^0) for iron (II) hexa-aza-macrocyclic complexes and the molecular model of electrocatalyst, and their respective demetallated forms in comparison with V_m and S_{298}^0 for already studied electrocatalysts

Compound, electrocatalyst	V_m (nm ³)		S_{298}^0 (J mol ⁻¹ K ⁻¹)	
	Compound or electrocatalyst	Demetallated form	Compound or electrocatalyst	Demetallated form
Fe ^(II) N ₄ [C ₂₀ N ₂ H ₁₂] ^a	0.439	0.419	396.8 ± 20	381.3 ± 20
Fe ^(II) N ₄ [C ₂₄ N ₂ H ₁₂] ^a	0.495	0.474	440.1 ± 22	423.9 ± 22
Fe ^(II) N ₄ [C ₅₈ N ₂ H ₂₀] ^a (electrocatalyst modeled in this work, Fe ^(II) N ₍₄₊₂₎ /C)	1.007	0.987	836.4 ± 27	820.9 ± 27
Fe ^(II) N ₍₂₊₂₎ /C (“armchair” electrocatalyst) ^b	1.011	0.986	839.5 ± 27	820.2 ± 27
Fe ^(II) N ₄ /C (“zig-zag” electrocatalyst) ^b	1.049	1.029	868.9 ± 27	853.5 ± 27

^aFigures 1–3A.

^bRef. [50]

TABLE 3 Thermodynamic data for several ions, the values of Fe–N bond energy for iron (II) hexa-aza-macrocyclic complexes and the modeled electrocatalysts, and N–H bond energy in the demetallated frameworks in comparison with the same data for already studied electrocatalysts

Ion, compound, electrocatalyst	$\Delta_f H_{298}^0$ (kJ mol ⁻¹)	S_{298}^0 (J K ⁻¹ mol ⁻¹)	$E_{\text{Fe-N}}$ (kJ mol ⁻¹)	$E_{\text{N-H}}$ ^a (kJ mol ⁻¹)
H _(aq) ⁺	0 ^b	0 ^b	–	–
Fe _(aq) ²⁺	–92.5 ± 0.84 ^b	–101.6 ± 3.7 ^b	–	–
Fe ^(II) N ₄ [C ₂₀ N ₂ H ₁₂]	Use $E_{\text{Fe-N}}$	396.8 ± 20	219.4 ± 5	382.3 ± 4
Fe ^(II) N ₄ [C ₂₄ N ₂ H ₁₂]	Use $E_{\text{Fe-N}}$	440.1 ± 22	219.4 ± 5	382.3 ± 4
Fe ^(II) N ₄ [C ₅₈ N ₂ H ₂₀] (electrocatalyst modeled in this work, Fe ^(II) N ₍₄₊₂₎ /C)	Use $E_{\text{Fe-N}}$	836.4 ± 27	221.4 ± 5	382.3 ± 4
Fe ^(II) N ₍₂₊₂₎ /C (“armchair” electrocatalyst) ^c	Use $E_{\text{Fe-N}}$	839.5 ± 27 ^c	216.3 ± 5	use $E_{\text{H}^+\dots\text{N}}$ ^d 190.0 ± 5 ^e
Fe ^(II) N ₄ /C (“zig-zag” electrocatalyst) ^c	Use $E_{\text{Fe-N}}$	868.9 ± 27 ^c	216.3 ± 5	382.3 ± 4 ^c

^a $E_{\text{N-H}}$ in demetallated frameworks.

^bRef. [7]

^cRef. [50]

^d $E_{\text{H}^+\dots\text{N}}$ is the energy of H⁺⋯N coordination bond formed when H⁺ replaces Fe^(II) in FeN₍₂₊₂₎/C site (Ref. [50]).

^eOur estimation based on the back-calculations, this work (see also Ref. [57]).

constants for ions participating in Reactions (1)–(3), and Fe–N and N–H bond energies are given in Table 3.

Using data given in Tables 2 and 3, the enthalpy and entropy changes for Reactions (1)–(3) were calculated. Then, based on these values, the Gibbs free energies of Fe²⁺/H⁺ ion exchange (Reactions 1–3; acid leaching from iron (II) hexa-aza-macrocyclic complexes and the active site of the electrocatalyst) at 298 and 353 K (Equation 5) were assessed and, further, used for the estimation of equilibrium constants with Equation (4).

The summary on the thermodynamics of iron acid leaching from iron (II) complexes, the modeled electro-

catalyst and, for comparison, from several electrocatalysts already studied in Ref. [50] is presented in Table 4.

Here, it is also important to estimate the incertitude in calculating the equilibrium constants. Turning again to Equations (4) and (5), it can be seen that the incertitude in calculating the equilibrium constants will depend on the errors in determining enthalpy and entropy change of the reactions of demetallation. As it was noted above, the error on values of the entropy changes of the reactions demetallation is low, since the same method is used in the estimations of S_{298}^0 of the product and reactant parts of these reactions. Therefore, the main contribution

TABLE 4 Summary on the thermodynamics of iron leaching ($\text{Fe}^{2+}/\text{H}^+$) from iron (II) hexa-aza-macrocyclic complexes and active sites of several electrocatalysts at 298 and 353 K in comparison with the same data for already studied electrocatalysts

Compound, electrocatalyst	Reaction of iron acid leaching	$\Delta_r H_{298}^0$ (kJ mol ⁻¹)	$\Delta_r S_{298}^0$ (J mol ⁻¹ K ⁻¹)	K_c at temperature T (K)	
				298	353
$\text{Fe}^{(\text{II})}\text{N}_4[\text{C}_{20}\text{N}_2\text{H}_{12}]$	Equation (1)	20.5	-117.1	1.95×10^{-10}	7.07×10^{-10}
$\text{Fe}^{(\text{II})}\text{N}_4[\text{C}_{24}\text{N}_2\text{H}_{12}]$	Equation (2)	20.5	-117.8	1.79×10^{-10}	6.50×10^{-10}
$\text{Fe}^{(\text{II})}\text{N}_4[\text{C}_{58}\text{N}_2\text{H}_{20}]$ (electrocatalyst modeled in this work, $\text{Fe}^{(\text{II})}\text{N}_{(4+2)}/\text{C}$)	Equation (3)	28.5	-117.1	7.71×10^{-12}	4.61×10^{-11}
$\text{Fe}^{(\text{II})}\text{N}_4[\text{C}_{62}\text{H}_{22}]$ (“zig-zag” modeled electrocatalyst, $\text{Fe}^{(\text{II})}\text{N}_4/\text{C}$)	–	7.9	-116.1	3.6×10^{-8}	5.8×10^{-8}
$\text{Fe}^{(\text{II})}\text{N}_{(2+2)}[\text{C}_{60}\text{H}_{20}]$ (“armchair” modeled electrocatalyst, $\text{Fe}^{(\text{II})}\text{N}_{(2+2)}/\text{C}$)	–	10.7	-120.9	6.4×10^{-9}	1.3×10^{-8}

to the incertitude in estimating the equilibrium constants belongs to errors associated with the determination of the enthalpy of reactions, which, in turn, depend on the inaccuracies in estimating the Fe–N bond energies.

For example, three different methods for the assessment of Fe–N bond energy for the “zig-zag” modeled electrocatalyst yielded the following values in kJ mol⁻¹: 216.3 (this work), 213.5 (using correlation of the type “bond length–bond energy”, Ref. [50]), and 215.2 (using correlation of the type “bond order–bond energy”, Ref. [50]). The mean value is equal to 215.0 ± 1.4 kJ mol⁻¹. Using this value, we get for the equilibrium constant at 353 K the value $K_c = 3.2 \times 10^{-7}$. When comparing this value with the data given in Table 4 and Ref. [50] this means that our calculations are characterized by the incertitude which is equal to ± 1 order of magnitude, the accuracy, as we believe, unattainable using quantum-chemical methods (see Ref. [57]).

4 | DISCUSSION

4.1 | Stability toward demetallation in acid medium of the Fe-hexa-aza active sites

As can be seen by comparing the values of equilibrium constants, all studied iron (II) hexa-aza complexes and the hexa-aza active site of the modeled electrocatalyst are stable in an acid environment. A site is unstable if the quantity ($-RT \ln K_c$) < 0. As an example, for the active site of the modeled $\text{Fe}^{(\text{II})}\text{N}_{(4+2)}/\text{C}$ electrocatalyst, this quantity at 353 K is equal to $-8.314 \times 353 \times \ln(4.61 \times 10^{-11}) = 69\,850$ J mol⁻¹, that is, this site is stable. Among iron (II) hexa-aza complexes, the iron (II) complex with an hexa-aza-macrocyclic ligand having Phen groups (Figure 2A) is, apparently, slightly more stable than the iron (II) complex with an hexa-aza-macrocyclic ligand

having 2,2'-bipyridine groups (Figure 1A). Comparing the stabilities toward demetallation of the hexa-aza active site $\text{Fe}^{(\text{II})}\text{N}_{(4+2)}/\text{C}$ with the active sites of the FeN_4/C (“zig-zag”) and $\text{FeN}_{(2+2)}/\text{C}$ (“armchair”) electrocatalysts (Table 4, rows 4 and 5), it can be seen that the stability of the modeled hexa-aza electrocatalyst is about two to three orders of magnitude higher (since its K_c value is two to three orders of magnitude smaller) than the previously studied Fe-based “zig-zag” or “armchair” electrocatalysts. This difference is essential due to the $\Delta_r H_{298}^0$ of the demetallation reaction (Table 4), which is much more endothermic for $\text{FeN}_{(4+2)}/\text{C}$ with its two more nitrogen atoms in their electrocatalytic moiety than for the corresponding moieties of FeN_4/C or $\text{FeN}_{(2+2)}/\text{C}$ electrocatalyst (Table 4). Indeed, $\Delta_r H_{298}^0$ depends on the value of $E_{\text{Fe-N}}$, which itself is greatly affected by the value of $d_{\text{Fe-N}}$ (Equation 6). Shorter is the $d_{\text{Fe-N}}$, smaller is K_c and larger becomes the resistance to demetallation of the considered catalyst. However, for the hexa-aza $\text{FeN}_{(4+2)}/\text{C}$ catalyst, it is also clear in our opinion that an additional stabilization of its active site can be attributed to the two N-atoms of the second coordination sphere leading to the appropriate redistribution of the electron density in this electrocatalyst, increasing, as it was suggested above, the ionicity of the Fe–N bonds, and correspondingly $E_{\text{Fe-N}}$, the Fe–N bond strength (Equation 6).

4.2 | Estimation of the amount of iron ions leaching from the electrocatalysts at 353 K (80°C)

It is of practical interest to estimate the amount of iron ions leaching from the electrocatalysts in an acid medium at equilibrium conditions. This estimation is performed based on the following facts and assumptions: (i) the

experimentally determined activity of H^+ ions in Nafion at 353 K is equal to 2.14 (extrapolated value from Ref. [58]); (ii) the coefficient of activity of Fe^{2+} ions, due to the very low value of the equilibrium constant, can be taken equal to 1, meaning that $a_{Fe^{2+}} = c_{Fe^{2+}}$; (iii) the activity of the solid phases like $Fe^{(II)}N_4[C_{58}N_2H_{20}]$ and $H_2N_4[C_{58}N_2H_{20}]$ for Fe-based and demetallated hexa-aza catalysts, respectively, is equal to 1, by definition. Then, the expression for the constant of equilibrium, K_c , in terms of activities (or molar concentrations, if the coefficient of activity = 1) has the following form:

$$K_c = \frac{c_{Fe^{2+}}}{[a_{H^+}]^2} \quad (15)$$

where $c_{Fe^{2+}}$ and a_{H^+} are the equilibrium concentration ($mol\ L^{-1}$) of iron ions and activity of hydrogen ions, respectively. Using this equation, the concentration of interest of iron ions ($mol\ L^{-1}$ or $g\ L^{-1}$) can be easily determined. Thus, by substitution of K_c value at 353 K, which is equal to 4.61×10^{-11} (Table 4), and $a_{H^+} = 2.14$ into Equation (15), the equilibrium concentration of iron ions, as the result of Fe^{2+}/H^+ exchange in the modeled $Fe^{(II)}N_4[C_{58}N_2H_{20}]$ electrocatalyst, was obtained to be equal to $2.11 \times 10^{-10}\ mol\ L^{-1}$ or $1.18 \times 10^{-8}\ g\ L^{-1}$.

In the case of previously studied electrocatalysts (Table 4), the values of Fe^{2+} ions equilibrium concentration at 353 K are calculated equal to $2.7 \times 10^{-7}\ mol\ L^{-1}$ or $1.58 \times 10^{-5}\ g\ L^{-1}$ (“zig-zag” electrocatalyst) and 3.07×10^{-8} or $1.71 \times 10^{-6}\ g\ L^{-1}$ (“armchair” electrocatalyst).

As can be seen by comparing the calculated values, the extent of acid iron leaching from active sites of the modeled hexa-aza electrocatalyst is significantly lower than from the “zig-zag” and “armchair” FeN_4 site electrocatalysts. This lower iron leaching in acid is in agreement with the greater stability experimentally established for the 14-membered hexa-aza macrocyclic complex in comparison with the electrocatalyst based on Fe-phthalocyanine (FePc).¹ To be able to obtain electrochemical results, both the 14-membered un-pyrolyzed hexa-aza and FePc complexes were impregnated on carbon black (/C). They were then cycled between 0 and 1 V in O_2 -saturated acid (0.5 M H_2SO_4) solution.

4.3 | Discussion about the value of d_{Fe-N} used to calculate K_c for the $Fe^{(II)}$ hexa-aza catalytic site

So far, two main groups have synthesized and characterized several Fe-based hexa-aza molecular complexes in order to find similarities with some structural and electro-

chemical properties of pyrolyzed Fe–N–C catalysts. These new hexa-aza molecules are depicted in Figure 4. The synthesis of A1, A2, and A3 is described in Ref. [59] while that of B1, B2, and B3 is described in Ref. [2]. The targeted molecule for both groups was Tw2, which was the starting point of the thermodynamic calculations presented in this work. The starting complex for the synthesis of the two groups was the same demetallated hexa-aza complex: A1 or B1, which is also the same demetallated hexa-aza complex (Tw1) used in our calculations.

It is important to note that none of the synthetic attempts succeeded in synthesizing the targeted $Fe^{(II)}$ complex depicted as Tw2. Instead, all the syntheses ended up with $Fe^{(III)}$ hexa-aza complexes, even for A2, contrary to what was declared by the authors of that particular synthesis.⁵⁹ To obtain the Fe formal oxidation value of their A2 and A3 complexes, the latter authors compared the energy at 0.5 of their normalized XANES X-ray absorption spectra (that we will name $y(eV)$ for short) with that of a series of 10 Fe-based materials for which the formal oxidation state is supposed to be known. To help the reader with the conclusions of this comparison, the results are illustrated in Figure S1B. In that figure, one sees that $y(eV)$ for A3 falls in the middle of all reference materials identified to a Fe formal valence of +3 (including for FeTPPCl, the un-identified red point marked by an arrow in Figure S1B), while complex A2 was identified by the same authors as displaying a Fe formal valence of +2. This is mainly because FePc was misplaced. It was, indeed, attributed to the same $y(eV)$ value as that of FeTPPCl (a $Fe^{(III)}$ complex) and placed above Fe_3O_4 , which has two Fe ions in the +3 oxidation state and only one in the +2 oxidation state, and for which, the Fe formal valence of is $2^{2/3+}$. It is indeed known that, if the Fe ion is initially $Fe^{(II)}$ in a fresh synthesized FePc, it is gradually oxidized to $Fe^{(III)}$ in contact with air.⁶⁰ This gradual oxidation of the Fe ion is much more obvious at the $2p^{3/2}$ -edge than at the K-edge used in Ref. [59]. Therefore, the synthesis of all model complexes A2, A3, B2, and B3 yielded $Fe^{(III)}$ complexes. This explains why A2 and A3 have practically the same d_{Fe-N} value of 1.89 and 1.90 Å, respectively. It does not explain, however, the value of $1.97 \pm 0.08\ \text{Å}$ for B3. In this case, it was mentioned by the authors of B3 synthesis that the Fe ions in the μ -oxo hexa-aza complex B3 were puckered, meaning that they were displaced out of the plane of the four proximal N-atoms in the direction of μ -oxygen, which is holding the two macrocycles together. When $Fe^{(III)}$ is in the plane of the four proximal N-atoms of the hexa-aza macrocycle, as it is for A2 or A3, the Fe–N bond is much shorter. This was confirmed by Density Functional Theory (DFT) calculations performed on B4, for which a value of $d_{Fe-N} = 1.86\ \text{Å}$ was found, in agreement with the experimental Fe–N bond distance determined for A2 and A3.

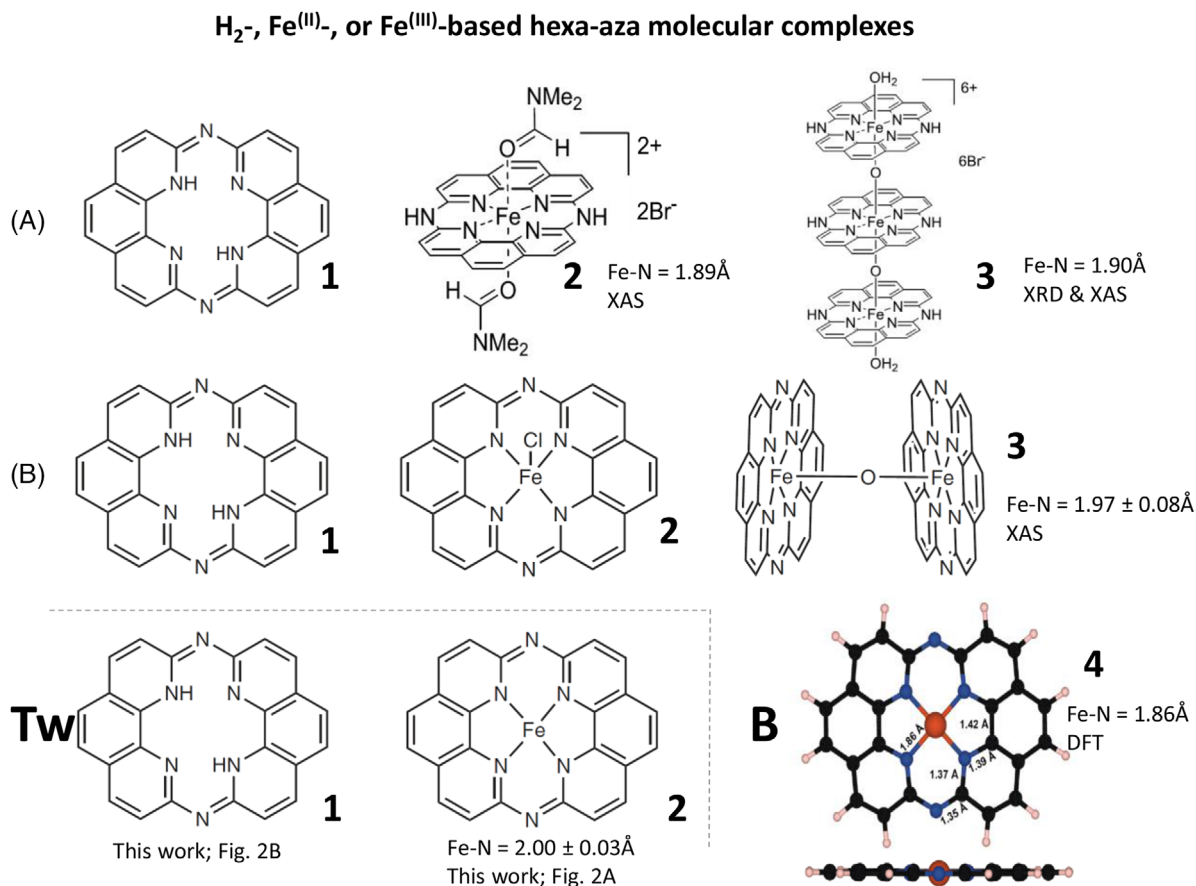


FIGURE 4 H₂⁻, Fe^(II)-, or Fe^(III)-based hexa-aza molecular complexes that have been characterized in the literature and in this work in the frame of their potential oxygen reduction reaction (ORR) catalytic properties. In Ref. [59] A1, A2, and A3 were named H₂HAM, Fe(H₂HAM)(DMF)₂Br₂, and [(H₂O)(Fe(H₂HAM)(μ-O)(Fe(H₂HAM)(μ-O)(Fe(H₂HAM)(H₂O)Br₆), respectively; in Ref. [2] B1, B2, B3, and B4 were named (phen₂N₂)H₂, (phen₂N₂)FeCl, [(phen₂N₂)Fe]₂O, and [(phen₂N₂)FeIII]⁺ (top and side views), respectively. In this work, Tw1 and Tw2 have been named H₂N₄[C₂₄N₂H₁₂] (depicted in Figure 2B), and FeN₄[C₂₄N₂H₁₂] (depicted in Figure 2A), respectively. The figure reports $d_{\text{Fe-N}}$ values (in Å) available for these complexes, as well as which techniques [X-ray diffraction (XRD) or X-ray absorption spectroscopy (XAS)] or procedure [density functional theory (DFT) or thermodynamic calculations (this work)] that were used to obtain these values

To continue our discussion, we have now to introduce an observation that was made for the porphyrin-based site (Fe^(II)N₄/C) belonging in Table 4 to the zig-zag modulated electrocatalyst. In order to explain the changes of the XANES spectrum at the Fe K-edge of Fe^(II)N₄/C with the applied potential, it was proposed that the Fe^(II) ion, which was measured at a distance of 2.7 Å, out of the plane of the four N-atoms of the site, was now measured at a Fe-N distance of 1.99–2.01 Å, in plane, when Fe^(II)N₄/C was electrochemically oxidized to Fe^(III)N₄/C.^{61,62} The porphyrinic Fe^(II)N₄/C site displays strong structural similarities with the Fe^(II)N₍₄₊₂₎/C hexa-aza site. They are both electrically neutral. Both are also conjugated sites integrated in the conjugation of their supporting graphene layer, either metallated or demetallated. It means that when the Fe²⁺ ion is leached out these sites, it is replaced with two H⁺ to maintain the electrical neutrality, without perturbing the neighboring conjugation. In other words,

upon leaching a Fe²⁺ ion, Tw2 in Figure 4 becomes Tw1.^{63–66}

We are proposing here that what happens to Fe^(II)N₄/C upon iron oxidation, may also happen to Fe^(II)N₍₄₊₂₎/C; that is, a change of the $d_{\text{Fe-N}}$ bond length distance upon oxidation to Fe^(III)N₍₄₊₂₎/C. A $d_{\text{Fe-N}}$ distance of 1.99 ± 0.03 Å was calculated in this work for Fe^(II)N₍₄₊₂₎/C. Accordingly, we are proposing that $d_{\text{Fe-N}}$ for Fe^(III)N₍₄₊₂₎/C is of the order of 1.90 Å, as it is experimentally observed for the Fe^(III) hexa-aza macrocycles when the Fe^(III) ion is in the plane of the four proximal N-atoms of A3.⁵⁹ The difference in the Fe-N bond length for Fe^(II)N₍₄₊₂₎/C upon a change in the iron oxidation state between its two positions in the site is 0.6–1.2 Å, while it is 0.6–0.8 Å, upon the change in the oxidation state of FeN₄/C. Consequently, FeN₍₄₊₂₎/C is vulnerable to demetallation in acid medium when it is in the reduced Fe^(II)N₍₄₊₂₎/C with $d_{\text{Fe-N}} = 1.99 \pm 0.03$ Å and it is the reduced form of Fe in the site that is considered in

the demetallation Equation (3) and for Equations (1) and (2) for the two hexa-aza molecular models as well as for the other two sites ($\text{Fe}^{\text{II}}\text{N}_{(2+2)}/\text{C}$ armchair and $\text{Fe}^{\text{II}}\text{N}_4/\text{C}$ zig-zag) reported in Table 4.

4.4 | How would a Fe-hexa-aza active site fit among the various active sites already proposed to perform ORR in electrocatalysts obtained after a high-temperature pyrolysis step?

Since the synthesis of the first ORR electrocatalyst obtained after a pyrolysis step of iron and nitrogen precursors impregnated on carbon, the scientific community has always been interested in the structure of the obtained molecular catalytic sites.

van Veen et al.,⁶⁷ who worked with a Fe-porphyrin impregnated on carbon black, defended the thesis that, after a high-temperature heat-treatment, the FeN_4 moiety of the porphyrin remained intact, and that after binding to the carbon support, FeN_4 was the center of the ORR catalytic site. This was clearly expressed in their review published in 1988, but it was only in 2002 that they published an image of their proposed catalytic site.⁶⁸ This representation is shown in Figure 5A. Eight bonds were left dangling as they did not know how the FeN_4/C site was connected to the carbon support. It is important to note that in FeN_4/C , all four N-atoms are of pyrrolic type. Therefore, FeN_4/C is an electrically neutral site. After demetallation, the Fe^{2+} ion is replaced by two H^+ .

At the same time, Yeager and coworkers also worked with Fe-porphyrin. However, they defended the idea that iron was reduced to iron metal during pyrolysis and it was iron metal that oxidized and was released as Fe ions in contact with an acidic medium. These Fe ions were captured by N-atoms (especially pyridinic ones) at the surface of the pyrolyzed carbon support to form ORR catalytic sites.⁶⁹ Yeager and coworkers⁷⁰ continued to defend the same idea about the catalytic sites even after having shown that metal macrocycles were not indispensable to the formation of ORR catalytic sites and that, pyrolyzing an inorganic metal precursor and a nitrogen precursor impregnated on carbon black also produced ORR active FeN_x sites. In 2007, we demonstrated at Institut National de la Recherche Scientifique (INRS) that the FeN_x site proposed by Yeager was only a precursor of a much more active site obtained after another high-temperature pyrolysis.⁷¹

In 2002,⁷² we also demonstrated by time of flight secondary ion mass spectroscopy (ToF SIMS) analysis of ORR Fe-based catalysts that, whatever was the starting iron precursor (a Fe-porphyrin or an inorganic salt-like Fe-acetate), two ORR catalytic sites were always simulta-

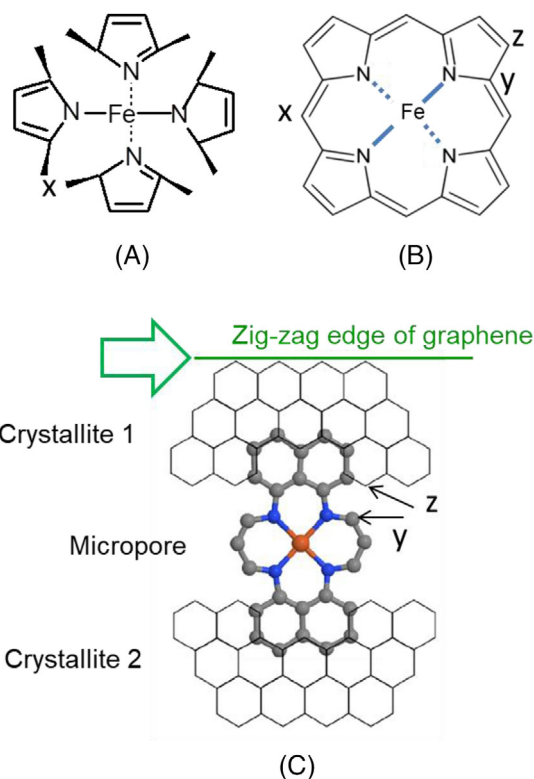


FIGURE 5 First representation of the FeN_4/C catalytic site, according to van Veen and coworkers⁶⁸ (A); structure of the Fe-porphyrin (B); structure proposed in Figure S14 of Ref. [49] for $\text{FeN}_4\text{C}_{12}$ “representing the zig-zag edge graphene sheet generated by adding C_6 rings to the Fe–N–C porphyrinic active site” (C). In our nomenclature, “C” is a developed representation of the FeN_4/C site, bridging two zig-zag edges of graphitic crystallites across a micropore of the carbon support

neously obtained; one site was identified by its FeN_2C_4^+ ion signature (see Figure 6A). It was the main ion collected in the family composed of FeN_2C_y^+ ions, and another site identified by its FeN_4C_8^+ signature (see Figure 6B), which was the main ion collected in the family composed of FeN_4C_y^+ ions, as well as some fragments of FeN_4C_y^+ collected in the FeN_3C_y^+ and FeN_1C_y^+ ion families. At that time, we assigned the FeN_4C_8^+ ion to the van Veen FeN_4/C site and tentatively attributed the FeN_2C_4^+ ion to a FeN_2/C site for which the two N-atoms were of pyridinic character. We knew, of course, that the FeN_2/C structure was incomplete.

After a few years of gathering other information about the simultaneous presence of two active sites in the catalysts, we also knew⁷³: (i) that the catalytic activity increased when the N-content of the carbon support increased; (ii) that the Fe in the site was always a Fe ion; (iii) that most active sites were located in micropores; (iv) that Mössbauer and extended X-ray absorption fine structure spectroscopies of Fe-based catalysts mainly detected four N-atoms in close proximity of the Fe ion in the site.

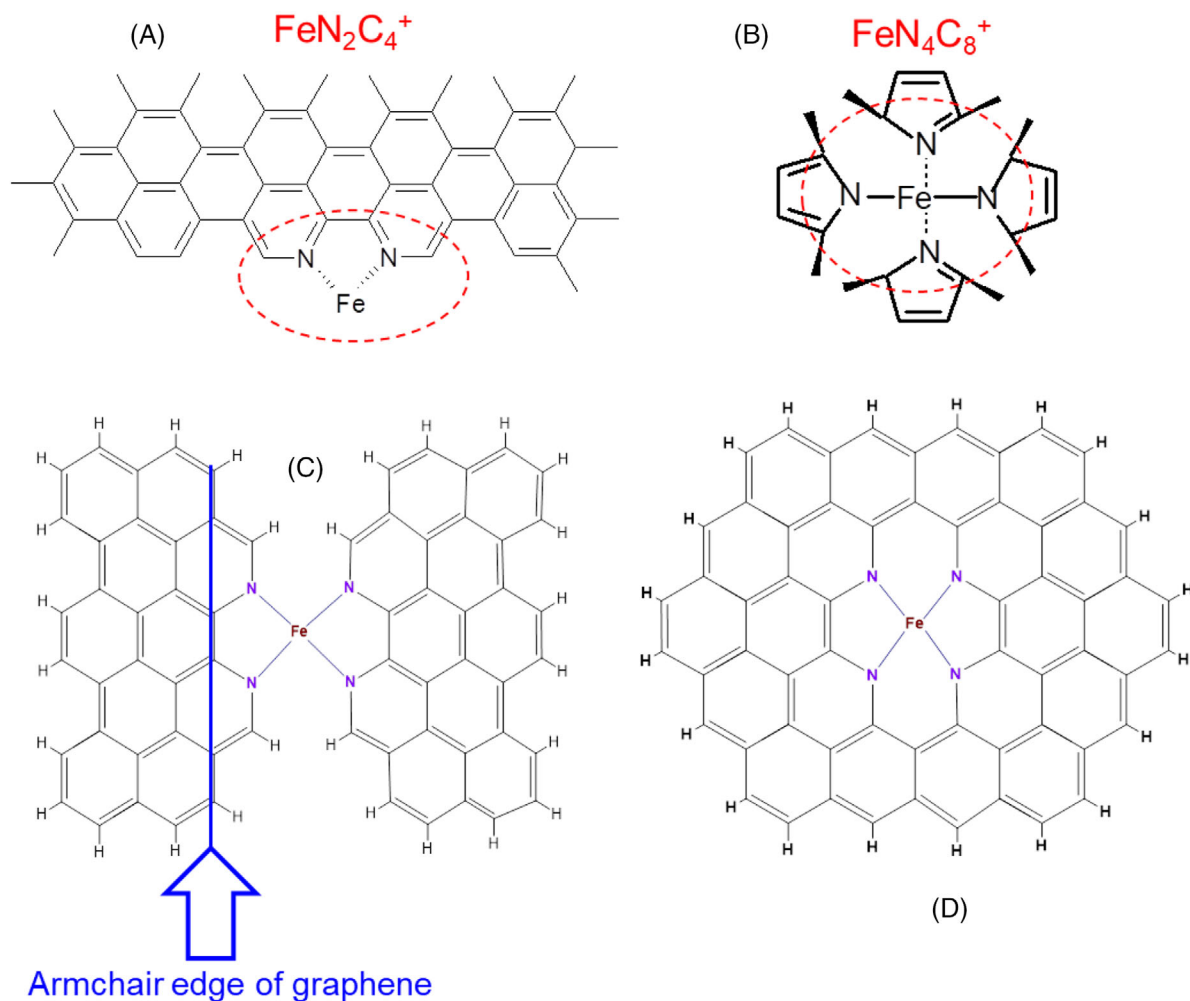


FIGURE 6 FeN_2C_4^+ ion (A), identified by ToF SIMS⁷² as the signature of the $\text{FeN}_{(2+2)}/\text{C}$ site represented in (C), bridging a micropore, and in (D), embedded in a graphene layer; FeN_4C_8^+ ion (B), identified by ToF SIMS⁷² in the same catalyst than FeN_2C_4^+ . FeN_4C_8^+ is the ToF SIMS signature⁷² of the van Veen FeN_4/C site illustrated in Figure 5

Thus, we proposed the two following structures for the active sites simultaneously detected in all Fe-based catalysts obtained by pyrolysis: the first one was the van Veen type catalytic site with four pyrrolic-type N-atoms (illustrated in Figure 5A) and (ii), the second one was a new catalytic site that we named $\text{FeN}_{(2+2)}/\text{C}$, located in a micropore where the site bridges the edges of two graphitic crystallites with a Fe ion coordinated by four pyridinic-type nitrogen atoms (see Figure 15 in Ref. [74] for the original figure and Figure 6C in this work). The $\text{FeN}_{(2+2)}/\text{C}$ site has been the subject of many DFT studies. So were also other sites of the same nature, but with fewer pyridinic nitrogen atoms in close vicinity with the Fe ion that renders these sites less stable, yet able to produce ORR.^{75–77} A particularity of the $\text{FeN}_{(2+2)}/\text{C}$ site is that it is easily embedded in a graphene layer (see Figure 6D). To form such a structure, one only has to complete the graphene structure which is missing in the micropore. This operation is much more difficult to perform for the FeN_4/C site, as embed-

ding the site necessitates the introduction in the graphene sheet of four Stone-Wales defects (one at each corner of the FeN_4/C site).⁷⁸ The existence of embedded $\text{FeN}_{(2+2)}/\text{C}$ sites has been proven by high-resolution transmission electron microscopy, which demonstrated that a graphene structure could be observed around the Fe ions.^{79–81}

Coordination complexes of Fe^{2+} with Phen exist with one, two, or three ligands.⁸² They all carry a (+2) charge since the two electrons of the pyridinic nitrogen atoms in the Phen molecule are non-bonding. It is, therefore, logical to deduce that $\text{FeN}_{(2+2)}/\text{C}$ sites are also positively charged by the positive charge of the Fe ion. One or two anions with an electrical neutralization charge per each $\text{FeN}_{(2+2)}/\text{C}$ site should therefore be part of these catalysts. This is practically never mentioned in the literature despite the fact that the negative charge density of these catalysts needs to compensate around $10^{19} \pm 1$ positively charged $\text{FeN}_{(2+2)}/\text{C}$ sites per gram of catalyst.⁸³ Always following the chemistry of $\text{Fe}(\text{Phen})_{1-3}^{2+}$ complexes, when a $\text{FeN}_{(2+2)}/\text{C}$ loses its Fe^{2+}

ion in an acidic medium, the latter is replaced by a single H^+ which coordinates to the four pyridinic nitrogen atoms⁵⁰.

In Figure 6C, one sees that the pyridinic N-atoms on each crystallite are located on the armchair edge of the graphene layer. $FeN_{(2+2)}/C$ sites will not be found on the zig-zag edge of the graphene layer, even if two pyridinic atoms are substituting for two carbons located on two neighboring cycles of the zig-zag edge. Not only, will these pyridinic atoms be too close to each other to support the site, but their non-bonding orbitals will not be directed at the appropriate angle to coordinate the Fe ion. Jaouen and coworkers⁴⁹ have, however, found that it is possible to use the zig-zag edge of graphene crystallites to anchor the van Veen FeN_4/C catalytic site. This is shown in Figure 5C. In order to go from Figure 5A to Figure 5C, the four pairs of dangling bonds in Figure 5A are joined in “x”, then Figure 5A is rotated 45° to obtain the same presentation as Figure 5B, which is the Fe-porphyrin structure. Figure 5B is then compared with Figure 5C to recognize that the Fe-porphyrin structure is indeed identified in Figure 5C once four C–C bonds have been established between “y” and “z.” Once completed, Figure 5C represents therefore the van Veen FeN_4/C site bridging two zig-zag edges of graphitic crystallites across a micropore of the carbon support.

In their work published in 2015, Jaouen and coworkers⁴⁹ named FeN_4C_{12} the site described in Figure 5C, since in that site the Fe ion is surrounded by 4 N-atoms and 12 proximal C-atoms. So far, we labeled that site: FeN_4/C . They also declared that FeN_4C_{12} was the only site present in their catalyst in contrast to a $FeN_{(2+2)}/C$ site structure (that they named $FeN_{2+2}C_{4+4}$ for the version bridging a micropore like in Figure 6C, or FeN_4C_{10} , for the embedded version like in Figure 6D) assumed hitherto (according to them) for pyrolyzed Fe–N–C materials. This did not prevent them to use a $FeN_{(2+2)}/C$ site structure in their contribution to another important work published in 2020 by Jia and coworkers,⁸⁴ describing the formation of ORR catalytic sites when a Fe-salt, a nitrogen precursor like Phen and a nitrogen and carbon precursor like zinc-imidazolate-framework-8 (ZIF-8) are heat-treated to obtain a Fe-based catalyst. In a more recent paper yet, published in 2021, Jaouen and coworkers⁸⁵ recognize that there are indeed two catalytic sites in Fe-based catalysts obtained by the pyrolysis of Fe-acetate, Phen, and ZIF-8. They are: (i) site S1 or FeN_4C_{12} (or FeN_4/C in our nomenclature) with four pyrrolic-type nitrogen atoms and characterized by a Mössbauer doublet D1. This site is not stable in PEM fuel cells as it demetallizes. After demetallation, the Fe^{2+} ion is first exchanged for H^+ with the proton exchanging Nafion material surrounding the catalyst, then gets oxidized as Fe^{3+} , which is found later on aggregated in Fe_2O_3 crystal-

lites in the cathode catalyst layer; (ii) site S2 or FeN_4C_{10} (or $FeN_{(2+2)}/C$ in our nomenclature) with four pyridinic-type nitrogen atoms characterized by a Mössbauer doublet D2. According to Jaouen and coworkers, this site is stable.

In the present discussion, we like to propose an alternative to the present assignment of the stable Fe-based site previously made in Ref. [85] According to the K_c values listed in Table 4 for FeN_4/C , $FeN_{(2+2)}/C$, and $FeN_{(4+2)}/C$, we propose that the stable site is not $FeN_{(2+2)}/C$, which has a K_c value for its thermodynamic demetallation similar to that of FeN_4/C , but it is $FeN_{(4+2)}/C$ instead, which displays (depending on the temperature) a K_c value between two to four orders of magnitude smaller than that of $FeN_{(2+2)}/C$ (or of FeN_4/C). The structure of $FeN_{(4+2)}/C$ is presented in Figure 3A. It differs from that of $FeN_{(2+2)}/C$ by only two supplementary N-atoms, whose particularity is to stabilize the $FeN_{(4+2)}/C$, against demetallation in acid medium as it was described in Section 4.1. It is also important to note that, alike FeN_4/C , $FeN_{(4+2)}/C$ is an electrically neutral site. When such a site demetallizes, the Fe^{2+} ion is replaced with two H^+ .^{63–66}

Nabae and coworkers have already proposed to replace FeN_4 sites with four pyridinic nitrogen atoms embedded in graphene (or $FeN_{(2+2)}/C$ armchair sites in our nomenclature) with a Fe-hexa-aza-type site. This is obvious from their graphical abstract in Ref. [59] This proposition has been later on¹ based on the high durability during ORR in acid solution of a 14-member hexa-aza macrocyclic Fe-complex (A3/C in Figure 4 of this work) compared with the ORR durability behavior of a 16-member Fe-based-phthalocyanine measured in the same solution. By determining K_c equilibrium values for the demetallation of $Fe^{(II)}N_4/C$, $Fe^{(II)}N_{(2+2)}/C$, and $Fe^{(II)}N_{(4+2)}/C$ catalytic sites in acid medium, we have now strengthened their proposition. Another element that argues in favor of a Fe-hexa-aza ORR catalytic site comes from the publication of Surendranath and coworkers.² For the hexa-aza molecules (B2 and B3 depicted in Figure 4) synthesized by this group,² the highlight in the comparison of both Fe–N–C catalysts and the synthesized molecules is not in the stability of B2 or B3 complexes during ORR, but rather in the Mössbauer properties of B2. Indeed, the important Mössbauer parameters, δ and Δ_{EQ} , of the doublet characterizing the Mössbauer spectrum of B2 are exactly the same as the corresponding δ (0.37 mm s⁻¹) and Δ_{EQ} (3.06 mm s⁻¹) parameters assigned to the doublet D2, reputed to be stable in the Mössbauer spectrum of Fe–N–C.⁸⁵ Fe–N–C also displays another doublet, D1, characterized by $\delta = 0.46$ mm s⁻¹ and $\Delta_{EQ} = 1.08$ mm s⁻¹,² usually assigned to FeN_4 with the four nitrogen atoms in a pyrrolic environment,^{2,49} and reputed to demetallate in Ref. [85] The existence of two Fe-based catalytic sites of different stabilities in fuel cells

for a catalyst made by the pyrolysis of a Fe-salt, Phen, and ZIF-8 as reported by INRS in 2011,⁸⁶ also perfectly agrees with the present conclusions. When this catalyst was maintained at a constant potential in PEM fuel cell, the current decay curve was showing a fast exponential decay followed by a much slower one.⁵ The fast decay was attributed to the demetallation of catalytic sites (that we know now to be FeN₄/C sites) located in the catalyst micropores. The much more stable site may now be attributed to hexa-aza FeN₍₄₊₂₎/C. Finally, the structures of a Fe-hexa-aza macrocycle of the FeN₍₄₊₂₎/C type and that of a pyrrolic FeN₄/C type were also proposed as potential active sites in Fe–N–C in a recent review by Zagal et al.⁸⁷

In the Fe-based catalysts, which are so far the most studied Pt-free ORR electrocatalysts in PEM fuel cells,^{88,89} we have therefore two Fe-based active catalytic sites: (i) FeN₄/C (or FeN₄C₁₂), which would be the most thermodynamically unstable site toward demetallation in acid medium; and (ii) FeN₍₄₊₂₎/C that would be a site much more stable in acid medium. Besides the two Fe-based sites, we have also some CN_x active sites. We have already shown that, above ~ 0.7 V, the contribution to the total current of the CN_x sites is negligible, but it represents about one-third of the total current at 0 V in H₂/O₂ PEM fuel cell.⁹⁰ Once FeN₄/C sites disappear by demetallation from the catalyst layer, the sites left that are able to generate ORR current are FeN₍₄₊₂₎/C and CN_x. If the FeN₍₄₊₂₎/C sites are indeed stable toward demetallation, the causes of catalyst instability degrading these remaining sites during the slow exponential decay in fuel cell, are either the electrochemical corrosion of the catalyst or its chemical corrosion by H₂O₂ (and its Fenton derivatives). We already demonstrated, on the one hand, that the electrochemical corrosion was becoming important only above ~ 0.7 V in PEM fuel cells.⁵ On the other hand, we ignore what is the H₂O₂ evolution yield as a function of the potential in fuel cells, but it increases below ~0.7 V in acid solution at pH 1.⁹⁰ The two effects may therefore cause the instability of the remaining active sites with relative importance varying with the applied fuel cell potential.

5 | CONCLUSIONS

In this work, we presented a thermodynamic assessment of the stability behavior in acid environment at 298 and 353 K of two iron (II) hexa-aza-macrocylic complexes and of an hexa-aza-iron-based (Fe^{II}N₍₄₊₂₎/C) potential active site for ORR in PEM fuel cells. The main conclusion arising from the thermodynamics study of the iron leaching from iron (II) hexa-aza complexes and the modeled hexa-aza electrocatalyst at both 298 and 353 K (80°C, being the usual running temperature of PEM fuel cells) is that:

- The studied iron (II) hexa-aza complexes and the hexa-aza active site of this type of electrocatalysts are chemically stable in an acid environment, considering that the equilibrium constants of their demetallation reactions are a criterium of their chemical stability.
- The stability of the modeled hexa-aza electrocatalyst is about two to four orders of magnitude higher (since its K_c value is two to four orders of magnitude smaller, depending on the temperature) than the previously studied Fe-based “zig-zag” or “armchair” electrocatalysts.
- This difference is essentially due to the $\Delta_r H_{298}^0$ of the demetallation reaction (Table 4), which is much more endothermic for FeN₍₄₊₂₎/C with its two supplementary nitrogen atoms in the electrocatalytic site than for the corresponding FeN₄/C or FeN₍₂₊₂₎/C sites (taking also into account that $\Delta_r S_{298}^0$ values for all the three studied electrocatalytic sites are very close; see Table 4).
- The equilibrium concentration of iron ions, as the result of Fe²⁺/H⁺ exchange in the modeled hexa-aza electrocatalyst, calculated for 353 K, is equal to about 2.1×10^{-10} mol L⁻¹ or 1.2×10^{-8} g L⁻¹. This is about two orders of magnitude smaller than for the previously studied Fe-based “zig-zag” or “armchair” electrocatalysts.
- Evidently, the latter fact is due to a specific chemical structure of the central part of the modeled site (Figure 3), which represents the structural motif of the hexa-aza-macrocylic complexes of Fe^(II) covalently bonded with carbon hexagons.
- The so-called chelate effect (due to high values of $T\Delta S$ in Equation 12) is also responsible for the stability of these types of electrocatalytic sites.
- The chemical stability of the modeled electrocatalytic site is valid for systems that are in the state of chemical equilibrium. But, under dynamic conditions, when Fe²⁺ ions exit the system (because they are exchanged with H⁺ in ion exchange membranes or they are leaving the cathode with the flow of water produced by the oxygen reduction in a running fuel cell), the progressive demetallation of the electrocatalytic sites can be conceivable, according to the Le Chatelier’s principle.

In this work, we have also discussed about the fit of the hexa-aza Fe^{II}N₍₄₊₂₎/C potential site among the other potential active sites that have already been proposed in the literature to be ORR active. More specifically we compared the structural and electrochemical properties of the Fe^{II}N₍₄₊₂₎/C hexa-aza potential site with the known structural and electrochemical properties of: (i) Fe^{II}N₄/C a molecular site essentially found in micropores where it is bridging the zig-zag edges of two graphene sheets and for which the four nitrogen atoms are of pyrrolic type, (ii) Fe^{II}N₍₂₊₂₎/C, a molecular site found either between

the armchair edges of two graphene sheets in a micropore or embedded in a graphene sheet of the catalyst and for which the four nitrogen are of pyridinic type. Our conclusions are that the two main Fe-based sites in Fe–N–C active catalysts for ORR are: (i) Fe^{II}N₄/C, and (ii) Fe^{II}N₍₄₊₂₎/C, the hexa-aza site, but not the usually considered Fe^{II}N₍₂₊₂₎/C. Fe^{II}N₄/C is more active but much less stable than Fe^{II}N₍₄₊₂₎/C in the acid medium of PEM fuel cells, in agreement with the literature. To these two Fe-based sites, it is still important to add the ORR contribution of CN_x sites that is low at high potential but becomes major at low potential.

ACKNOWLEDGMENTS

This work was supported by the Natural Sciences and Engineering Research Council of Canada (NSERC).

CONFLICT OF INTEREST

The authors declare no conflict of interest.

ORCID

Vassili P. Glibin  <https://orcid.org/0000-0003-3427-669X>
 Jean-Pol Dodelet  <https://orcid.org/0000-0002-4978-0218>
 Gaixia Zhang  <https://orcid.org/0000-0002-5340-8961>

REFERENCES

- Ohyama J, Moriya M, Takahama R, et al. High durability of a 14-membered hexaaza macrocyclic Fe complex for an acidic oxygen reduction reaction revealed by in situ XAS analysis. *JACS Au*. 2021;1(10):1798-1804.
- Marshall-Roth T, Libretto NJ, Wrobel AT, et al. A pyridinic Fe–N₄ macrocycle models the active sites in Fe/N-doped carbon electrocatalysts. *Nat Commun*. 2020;11(1):5283.
- Ferraudi G, Canales JC, Kharisov B, et al. Synthetic N-substituted metal aza-macrocyclic complexes: properties and applications. *J Coord Chem*. 2007;58(1):89-109.
- Isaacs M, Canales JC, Aguirre MJ, et al. Electrocatalytic reduction of CO₂ by aza-macrocyclic complexes of Ni(II), Co(II), and Cu(II). Theoretical contribution to probable mechanisms. *Inorg Chim Acta*. 2002;339:224-232.
- Chenitz R, Kramm UI, Lefevre M, et al. A specific demetalation of Fe–N₄ catalytic sites in the micropores of NC_Ar + NH₃ is at the origin of the initial activity loss of the highly active Fe/N/C catalyst used for the reduction of oxygen in PEM fuel cells. *Energy Environ Sci*. 2018;11:365-382.
- Puigdomènech I, Rard JA, Plyasunov AV, Grenthe I. *TDB-4 Temperature Corrections to Thermodynamic Data and Enthalpy Calculations*. Nuclear Energy Agency; 1999.
- Naumov GB, Ryzhenko BN, Khodakovskii IL, Barnes I, Speltz V. *Handbook of Thermodynamic Data*. Menlo Park, CA/Springfield, VA: U.S. Geological Survey, Water Resources Division; 1974.
- Batsanov SS. Calculating atomic charges in molecules and crystals by a new electronegativity equalization method. *J Mol Struct*. 2011;1006(1-3):223-226.
- Von Szentpály L. Studies on electronegativity equalization. *J Mol Struct: THEOCHEM*. 1991;233:71-81.
- Smith DW. A new method of estimating atomic charges by electronegativity equilibration. *J Chem Educ*. 1990;67(7):4.
- Smith DW. Group electronegativities from electronegativity equilibration applications to organic thermochemistry. *J Chem Soc Farad Trans*. 1998;94(2):201-205.
- Reed JL. Electronegativity and atomic charge. *J Chem Educ*. 1992;69(10):785.
- Bratsch SG. Revised Mulliken electronegativities. II. Applications and limitations. *J Chem Educ*. 1988;65(3):223.
- Mortier WJ, Ghosh SK, Shankar S. Electronegativity-equalization method for the calculation of atomic charges in molecules. *J Am Chem Soc*. 2002;108(15):4315-4320.
- Oliferenko AA, Palyulin VA, Pisarev SA, Neiman AV, Zefirov NS. Novel point charge models: reliable instruments for molecular electrostatics. *J Phys Org Chem*. 2001;14(6):355-369.
- Gasteiger J, Marsili M. Iterative partial equalization of orbital electronegativity—a rapid access to atomic charges. *Tetrahedron*. 1980;36(22):3219-3228.
- Bultinck P, Vanholme R, Popelier PLA, De Proft F, Geerlings P. High-speed calculation of AIM charges through the electronegativity equalization method. *J Phys Chem A*. 2004;108(46):10359-10366.
- Yang ZZ, Cui BQ. Atomic charge calculation of metallo-biomolecules in terms of the ABEEM method. *J Chem Theory Comput*. 2007;3(4):1561-1568.
- Reed JL. Electronegativity: coordination compounds. *J Phys Chem A*. 2003;107(41):8714-8722.
- Bergmann D, Hinze J. Electronegativity and molecular properties. *Angew Chem Int Ed Engl*. 1996;35(2):150-163.
- Hinze J. The concept of electronegativity of atoms in molecule. In: Maksič ZB, Orville-Thomas WJ, eds. *Pauling's Legacy: Modern Modelling of the Chemical Bond: Theoretical and Computational Chemistry*. 1999:189-212.
- Lang PF, Smith BC. Electronegativity effects and single covalent bond lengths of molecules in the gas phase. *Dalton Trans*. 2014;43(21):8016-8025.
- Bratsch SG. Calculation of heteronuclear single bond enthalpies from Pauling electronegativities. *Polyhedron*. 1984;7(18):1677-1685.
- Matcha RL. Theory of the chemical bond. 6. Accurate relationship between bond energies and electronegativity differences. *J Am Chem Soc*. 2002;105(15):4859-4862.
- Smith DW. A new approach to the relationship between bond energy and electronegativity. *Polyhedron*. 2007;26(2):519-523.
- Boudreaux EA. Calculations of bond dissociation energies. New select applications of an old method. *J Phys Chem A*. 2011;115(9):1713-1720.
- Reed JL. Electronegativity: proton affinity. *J Phys Chem*. 2002;98(41):10477-10483.
- Rayb NK, Samuels L, Parr RG. Studies of electronegativity equalization. *J Chem Phys*. 1979;70(8):3680-3684.
- Ghosh DC, Chakraborty T. Computation of the dipole moments of some heteronuclear diatomic molecules in terms of the revised electronegativity scale of Gordy. *J Mol Struct: THEOCHEM*. 2009;916(1-3):47-52.

30. Ferreira R. A zeroth-order approximation for bond energies, hybridization states, and bond ionicities. I. Diatomic molecules and AI-BI crystals. *J Phys Chem.* 2002;68(8):2240-2248.
31. Evans RS, Huheey JE. Electronegativity, acids, and bases—III. Calculation of energies associated with some hard and soft acid–base interactions. *J Inorg Nucl Chem.* 1970;32(3):777-793.
32. Urusov VS. Orbital electronegativity concept and its role in energetic crystal chemistry. *J Struct Chem.* 1994;35(1):101-114.
33. Pauling L. *The Nature of the Chemical Bond.* 3rd ed. Ithaca, New York: Cornell University Press; 1960.
34. Komorowski L. Hardness indices for free and bonded atoms. In: *Structure and Bonding.* Berlin, Heidelberg: Springer-Verlag; 1993:46-69.
35. Gopikrishnan CR, Jose D, Datta A. Electronic structure, lattice energies and Born exponents for alkali halides from first principles. *AIP Adv.* 2012;2(1):012131.
36. Sanderson RT. *Polar Covalence.* New York, London, Toronto: Academic Press; 1983.
37. Hodge CA. *Doctoral Dissertation.* Lubbock, TX, USA: Texas Tech University; 1979.
38. Parr RG, Donnelly RA, Levy M, Palke WE. Electronegativity: the density functional viewpoint. *J Chem Phys.* 1978;68(8):3801-3807.
39. Carver JC, Gray RC, Hercules DM. Remote inductive effects evaluated by X-ray photoelectron spectroscopy (ESCA). *J Am Chem Soc.* 2002;96(22):6851-6856.
40. Huheey JE, Keiter EA, Keiter RL. *Inorganic Chemistry: Principles of Structure and Reactivity.* 4th ed. New York: Pearson; 1993.
41. Sanderson RT. Principles of Electronegativity: part 1. General Nature. In: *Simple Inorganic Substances.* Malabar, FL: Krieger Publishing Co Inc.; 1989.
42. Mulliken RS. A new electroaffinity scale; together with data on valence states and on valence ionization potentials and electron affinities. *J Chem Phys.* 1934;2(11):782-793.
43. Pearson RG. Absolute electronegativity and hardness: application to inorganic chemistry. *Inorg Chem.* 2002;27(4):734-740.
44. Komorowski L. Electronegativity and hardness in the chemical approximation. *Chem Phys.* 1987;114(1):55-71.
45. Bratsch SG. Revised Mulliken electronegativities: I. Calculation and conversion to Pauling units. *J Chem Educ.* 1988;65(1):34.
46. Hinze J, Jaffé HH. Electronegativity: III. Orbital electronegativities and electron affinities of transition metals. *Canad J Chem.* 1963;41(5):1315-1328.
47. Herrick DR. Connecting Pauling and Mulliken electronegativities. *J Chem Theory Comput.* 2005;1(2):255-260.
48. Cordero B, Gomez V, Platero-Prats AE, et al. Covalent radii revisited. *Dalton Trans.* 2008;(21):2832-2838.
49. Zitolo A, Goellner V, Armel V, et al. Identification of catalytic sites for oxygen reduction in iron- and nitrogen-doped graphene materials. *Nat Mater.* 2015;14(9):937-942.
50. Glibin VP, Dodelet J-P. Thermodynamic stability in acid media of FeN₄-based catalytic sites used for the reaction of oxygen reduction in PEM fuel cells. *J Electrochem Soc.* 2017;164(9):F948-F957.
51. Gingerich KA. Experimental and predicted stability of diatomic metals and metallic clusters. *Farad Symp Chem Soc.* 1980;14:109.
52. Van Hooydonk G. Calculation of bond energies in diatomic molecules. *Theor Chim Acta.* 1971;22(2):157-166.
53. Lin Y, Liu K, Chen K, et al. Tuning charge distribution of FeN₄ via external N for enhanced oxygen reduction reaction. *ACS Catal.* 2021;11(10):6304-6315.
54. Leroy G, Temsamani DR, Wilante C. Refinement and extension of the table of standard energies for bonds containing atoms of the fourth group of the periodic table. *J Mol Struct: THEOCHEM.* 1994;306(1):21-39.
55. Glasser L, Jenkins HDB. Standard absolute entropies, S°298, from volume or density. *Thermochim Acta.* 2004;414(2):125-130.
56. Hofmann DW. Fast estimation of crystal densities. *Acta Crystallogr B.* 2002;58(3):489-493.
57. Glibin V, Zhang G, Dodelet J-P, Sun S. Non-PGM electrocatalysts for PEM fuel cells: thermodynamic stability of potential ORR CoNx-C electrocatalytic sites. *J Electrochem Soc.* 2021;168(9):09450.
58. Umeda M, Sayama K, Maruta T, Inoue M. Proton activity of Nafion 117 membrane measured from potential difference of hydrogen electrodes. *Ionics.* 2012;19(4):623-627.
59. Moriya M, Takahama R, Kamoi K, et al. Fourteen-membered macrocyclic Fe complexes inspired by FeN₄-center-embedded graphene for oxygen reduction catalysis. *J Phys Chem C.* 2020;124(38):20730-20735.
60. Cook PL, Liu X, Yang W, Himpsel FJ. X-ray absorption spectroscopy of biomimetic dye molecules for solar cells. *J Chem Phys.* 2009;131(19):194701.
61. Li J, Ghoshal S, Liang W, et al. Structural and mechanistic basis for the high activity of Fe–N–C catalysts toward oxygen reduction. *Energy Environ Sci.* 2016;9:2418-2432.
62. Li J, Jaouen F. Structure and activity of metal-centered coordination sites in pyrolyzed metal–nitrogen–carbon catalysts for the electrochemical reduction of O₂. *Curr Opin Electrochem.* 2018;9:198-206.
63. Ogawa S, Yamaguchi T, Gotoh N. Synthesis of a novel macrocyclic compound and of its copper complex. *J Chem Soc Chem Commun.* 1972(10):577-578.
64. Ogawa S, Yamaguchi T, Gotoh N. Preparation of a conjugated tautomer of I, I 4 :7,8-diethenotetrapyrido- [2,1,6-de : 2',1',6'-gh : 2'',1'',6''-kl : 2''',1''',6'''-na] [1,3,5,8,10,12] hexa azacyclotetradecine and its metal derivatives. *J Chem Soc Perkin Trans I.* 1974:976-978.
65. Ogawa S. Preparation of macrocyclic compounds by thermal dimerization of 1, 10-phenanthroline derivatives. *J Chem Soc Perkin Trans I.* 1977:976-978.
66. Canales J, Ramirez J, Estiu G, Costamagna J. Bis-bipyridine hexa-aza-macrocyclic complexes of zinc(II) and nickel(II) and the catalytic reduction of carbon dioxide. *Polyhedron.* 2000;19(22-23):2373-2381.
67. van Veen JAR, Colijn HA, van Baar JF. On the effect of a heat treatment on the structure of carbon-supported metalloporphyrins and phthalocyanines. *Electrochim Acta.* 1988;33(6):801-804.
68. Bouwkamp-Wijnoltz AL, Visscher W, van Veen JAR, et al. On active-site heterogeneity in pyrolyzed carbon-supported iron porphyrin catalysts for the electrochemical reduction of oxygen: an in situ Mössbauer study. *J Phys Chem B.* 2002;106(50):12993-13001.
69. Scherson D, Tanaka AA, Gupta S, et al. Transition metal macrocycles supported on high area carbon: pyrolysis-mass spectrometry studies. *Electrochim Acta.* 1986;31(10):1247-1258.

70. Gupta S, Tryk D, Bae I, Aldred W, Yeager E. Heat-treated polyacrylonitrile-based catalysts for oxygen electroreduction. *J Appl Electrochem*. 1989;19(1):19-27.
71. Herranz J, Lefèvre M, Larouche N, Stansfield B, Dodelet J-P. Step-by-step synthesis of non-noble metal electrocatalysts for O₂ reduction under proton exchange membrane fuel cell conditions. *J Phys Chem C*. 2007;111(51):19033-19042.
72. Lefèvre M, Dodelet JP, Bertrand P. Molecular oxygen reduction in PEM fuel cells: evidence for the simultaneous presence of two active sites in Fe-based catalysts. *J Phys Chem B*. 2002;106(34):8705-8713.
73. Dodelet JP. The controversial role of the metal in Fe- or Co-based electrocatalysts for the oxygen reduction reaction in acid medium. In: Shao M, ed. *Electrocatalysis in Fuel Cells, A Non- and Low-Platinum Approach*. London: Springer-Verlag; 2013:271-338.
74. Charreteur F, Jaouen F, Ruggeri S, Dodelet JP. Fe/N/C non-precious catalysts for PEM fuel cells: influence of the structural parameters of pristine commercial carbon blacks on their activity for oxygen reduction. *Electrochim Acta*. 2008;53(6):2925-2938.
75. Kabir S, Artyushkova K, Kiefer B, Atanassov P. Computational and experimental evidence for a new TM-N₃/C moiety family in non-PGM electrocatalysts. *Phys Chem Chem Phys*. 2015;17(27):17785-17789.
76. Yang Y, Li K, Meng Y, Wang Y, Wu Z. A density functional study on the oxygen reduction reaction mechanism on FeN₂-doped graphene. *New J Chem*. 2018;42(9):6873-6879.
77. Cherif M, Dodelet JP, Zhang G, et al. Non-PGM electrocatalysts for PEM fuel cells: a DFT study on the effects of fluorination of FeN_x-doped and N-doped carbon catalysts. *Molecules*. 2021;26(23):7370.
78. Menga D, Low JL, Li YS, et al. Resolving the dilemma of Fe-N-C catalysts by the selective synthesis of tetrapyrrolic active sites via an imprinting strategy. *J Am Chem Soc*. 2021;143(43):18010-18019.
79. Deng D, Chen X, Yu L, et al. A single iron site confined in a graphene matrix for the catalytic oxidation of benzene at room temperature. *Sci Adv*. 2015;1(11):e1500462.
80. Chung HT, Cullen DA, Higgins D, et al. Direct atomic-level insight into the active sites of a high-performance PGM-free ORR catalyst. *Science*. 2017;357(6350):479-484.
81. Fei H, Dong J, Feng Y, et al. General synthesis and definitive structural identification of MN₄C₄ single-atom catalysts with tunable electrocatalytic activities. *Nat Catal*. 2018;1(1):63-72.
82. Irving H, Mellor DH. 1002. The stability of metal complexes of 1,10-phenanthroline and its analogues. Part I. 1,10-Phenanthroline and 2,2'-bipyridyl. *J Chem Soc*. 1962(0):5222-5237.
83. Zhang G, Yang X, Dubois M, et al. Non-PGM electrocatalysts for PEM fuel cells: effect of fluorination on the activity and stability of a highly active NC_{Ar} + NH₃ catalyst. *Energy Environ Sci*. 2019;12:3015-3037.
84. Li J, Jiao L, Wegener E, et al. Evolution pathway from iron compounds to FeI(II)-N₄ sites through gas-phase iron during pyrolysis. *J Am Chem Soc*. 2020;142(3):1417-1423.
85. Li J, Sougrati MT, Zitolo A, et al. Identification of durable and non-durable FeN_x sites in Fe-N-C materials for proton exchange membrane fuel cells. *Nat Catal*. 2020;4(1):10-19.
86. Proietti E, Jaouen F, Lefevre M, et al. Iron-based cathode catalyst with enhanced power density in polymer electrolyte membrane fuel cells. *Nat Commun*. 2011;2(1):416.
87. Zagal JH, Specchia S, Atanassov P. Mapping transition metal-MN₄ macrocyclic complex catalysts performance for the critical reactivity descriptors. *Curr Opin Electrochem*. 2021;27:100683.
88. He Y, Liu S, Priest C, Shi Q, Wu G. Atomically dispersed metal-nitrogen-carbon catalysts for fuel cells: advances in catalyst design, electrode performance, and durability improvement. *Chem Soc Rev*. 2020;49(11):3484-3524.
89. Osmieri L, Park J, Cullen DA, et al. Status and challenges for the application of platinum group metal-free catalysts in proton-exchange membrane fuel cells. *Curr Opin Electrochem*. 2021;25:100627.
90. Zhang G, Chenitz R, Lefèvre M, Sun S, Dodelet J-P. Is iron involved in the lack of stability of Fe/N/C electrocatalysts used to reduce oxygen at the cathode of PEM fuel cells? *Nano Energy*. 2016;29:111-125.

SUPPORTING INFORMATION

Additional supporting information can be found online in the Supporting Information section at the end of this article.

How to cite this article: Glibin VP, Dodelet J-P, Zhang G. Energetics and thermodynamic stability of potential Fe^(II)-hexa-aza-active sites for O₂ reduction in PEM fuel cells. *SusMat*. 2022;2:731-748. <https://doi.org/10.1002/sus2.94>